TOWARD GRAVITATIONAL WAVEFORMS FOR EXTREME AND INTERMEDIATE MASS RATIO INSPIRALS OF BLACK HOLE BINARY SYSTEMS: STRATEGIES FOR COMPUTING THE SELF-FORCE OF A SCALAR FIELD ON A SCHWARZSCHILD SPACETIME BACKGROUND DUE TO CAUSAL CONNECTIONS BETWEEN THE PARTICLE'S PAST ORBIT AND PRESENT POSITION USING THE DISCONTINUOUS GALERKIN, EFFECTIVE SOURCE, AND OSCULATING ORBIT METHODS

A Thesis/Dissertation

Submitted to the Graduate Faculty of the
Louisiana State University and
Agricultural and Mechanical College
in partial fulfillment of the
requirements for the degree of
Master of Science

in

Physics

by
Steven (Susan) Dorsher
B.S., Massachusetts Institute of Technology, 2004
M.S., The Ohio State University, 2006
M.S., University of Minnesota, 2013
December, 2017

Acknowledgments

I would like to thank Peter Diener and Frank Löffler for their guidance. Peter Diener especially has been very important to me, both as an advisor and personally. I would also like to thank Gabriela Gonzalez for the excellent opportunity to work on LIGO during the time of three detections, which provided me the funding I needed to continue the work detailed in this document. My parents, Paul and Joanne Dorsher, also deserve a mention, both for extraordinary moral support and for the financial support they provided that helped make this possible.

Table of Contents

List of Tables

List of Figures

Abstract

Insert the text of your abstract here. Make sure there is one blank line between the end of the Abstract text and the "end" command below to maintain double–spaced lines.

Chapter 1
Introduction

1.1 Gravitational Waves

On February 11, 2016, the LIGO Scientific Collaboration announced the first detection of gravitational waves from a black hole binary inspirals, occurring on September 14, 2015, with pre-merger masses of 36 $M_\odot$ and 29 $M_\odot$ and a post merger mass of 62 $M_\odot$ at a redshift of $z = 0.09$ [1]. Two subsequent detections followed, on December 26, 2015 [2] and on January 4, 2017 [3], with masses that are about the same to within an order of magnitude.

There is a question of what is meant, observationally, by a black hole. Does it need to have a horizon? Does it need to have a Kerr metric (the simplest possible space-time for a spinning black hole in general relativity)? Does it simply need to be a sufficiently compact object that it can't be ordinary nuclear matter? Historically, black holes have been defined by their compactness [15]; however, some studies are beginning to consider tests of horizons [] or of the Kerr metric itself [15]. X-ray binaries, gravitational wave constraints from binary-pulsar systems, active galactic nucleii models containing super-massive black holes on the order of $10^6 M_\odot$, and the three LIGO detections, as well as black hole formation models, suggest that black holes of all scales should be spinning [15]. However, for the purposes of this manuscript, I will consider non-spinning, spherically symmetric black holes in general relativity, described by the Schwarzschild metric.

Currently, there are four distinct windows on the gravitational wave universe planned or in progress. The Laser Interferometer Gravitational Wave Observatory, LIGO, probably deserves first listing, due to their recent success. LIGO observes gravitational waves using a ground based Michelson-Morley interferometer with two 4 kilometer long Fabry-Perot cavity arms. It detects strains as small as $10^-23 Hz^{-1/2}$ [16].

1.2 Extreme Mass Ratio Inspirals

1.3 EMRIs

1.4 The discontinuous galerkin method

1.5 LISA

Chapter 2
A simple numerical solution for a PDE using the Discontinuous Galerkin method

2.1 The Discontinuous Galerkin method

2.2 Separation of variables

2.3 Wave equation on flat spacetime

Chapter 3
A scalar field on a Schwarzschild background without a source

3.1 Scalar field on Schwarszchild spacetime

3.1.1 Multipole moment decomposition

3.1.2 Hyperboloidal compactification

Wave equation in this form Boundary conditions

3.1.3 Initial conditions

3.1.4 final results

Chapter 4
Elliptical orbits on a Schwarzschild spacetime

4.0.1 time dependent coordinate transformation

wave equation

4.0.2 effective source

4.0.3 orbital parameters (osculating orbits paper)

4.0.4 precession figure

chi(t),psir,psirtheta,psirphi,psirt

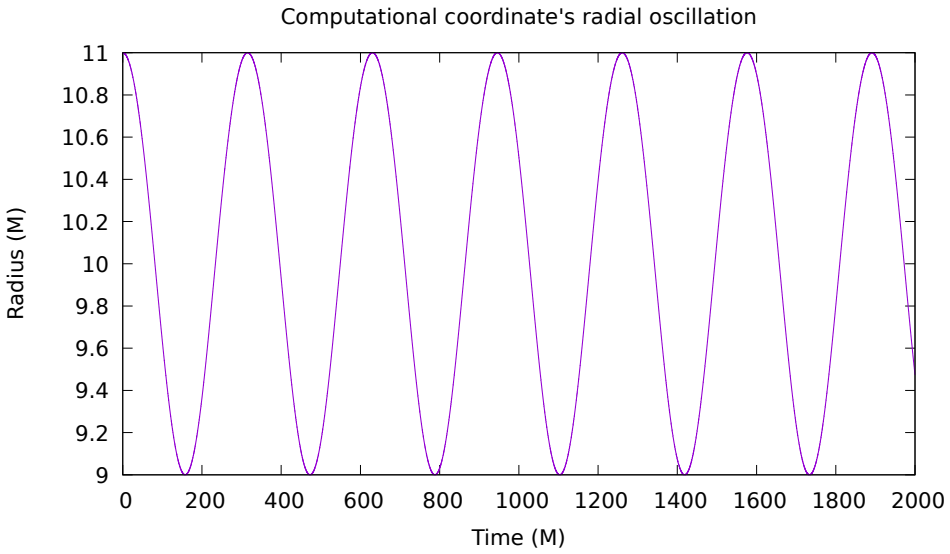

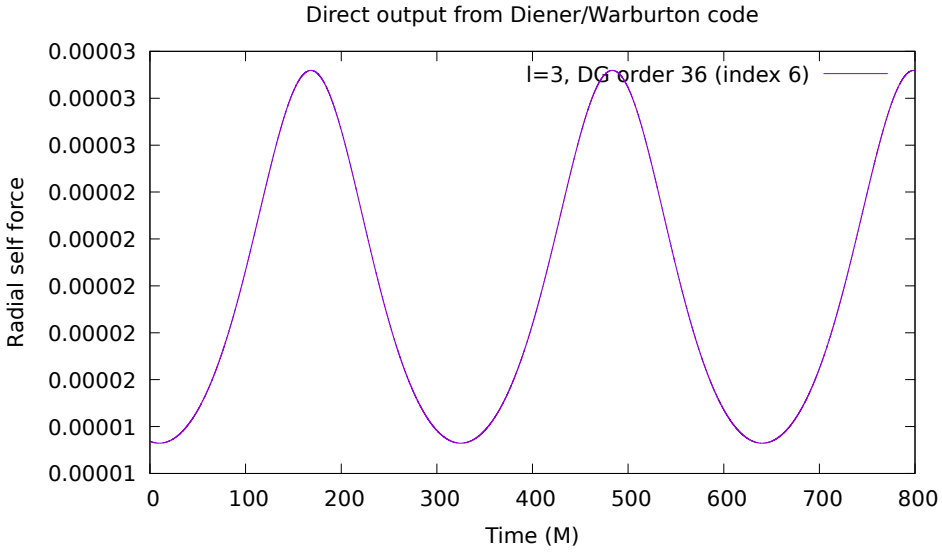

Figure 4.1: 470 M near perihelion, 640 M at aphelion

Chapter 5
Extrapolating the self force to infinite Disctontinuous Galerkin order

t472

5.1 l=2

5.1.1 Checking for discontinuities in $F_{\rm inf}$ for each each l-mode

There are no discontinuities in $F_{\rm inf}$ for any of the l-modes when the median approach is used. See mode zero for an example.

5.1.2 Determining $F_{\rm inf}$ using maximum likelihood fits to subsegments of lines in semilog space

Fit subsegments of lines in semilog space on DG order convergence plot after subtracting Finf for each possible starting order. pick starting order and starting and ending index of line segment with best possible chi-sq per dof (closest to one). use that finf. veto modes and starting indices that fail the alpha ratio test.

take standard deviation of surface plot as well as average.

Starting index	finf
2	4.18128309016e-05
3	mode failed
4	4.18128307505e-05
5	4.18128308245e-05
6	4.1812830828e-05

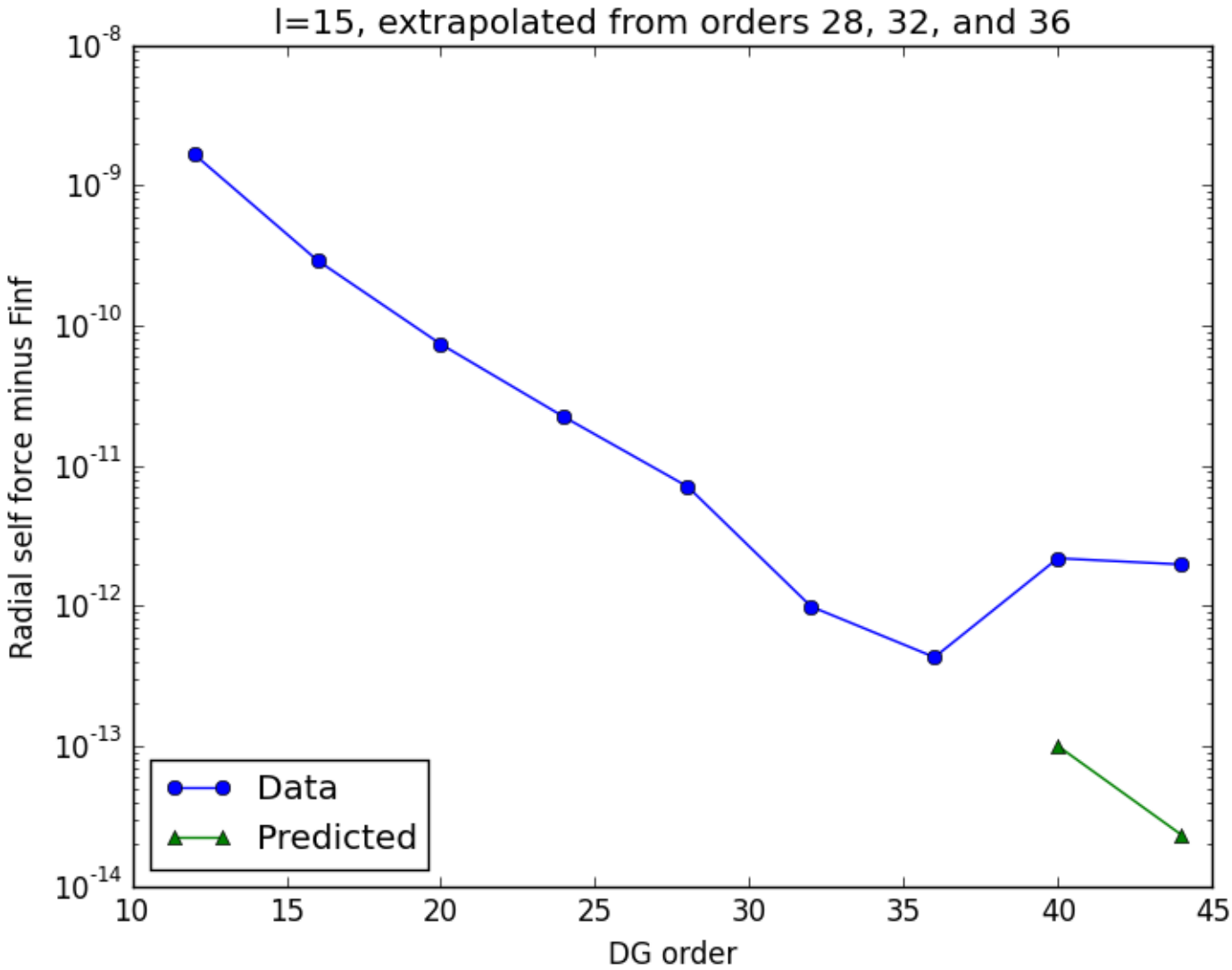
l=15, extrapolated from orders 28, 32, and 36
Radial self force minus Finf
DG order
Data
Predicted
10^-8
10^-9
10^-10
10^-11
10^-12
10^-13
10^-14
10
15
20
25
30
35
40
45

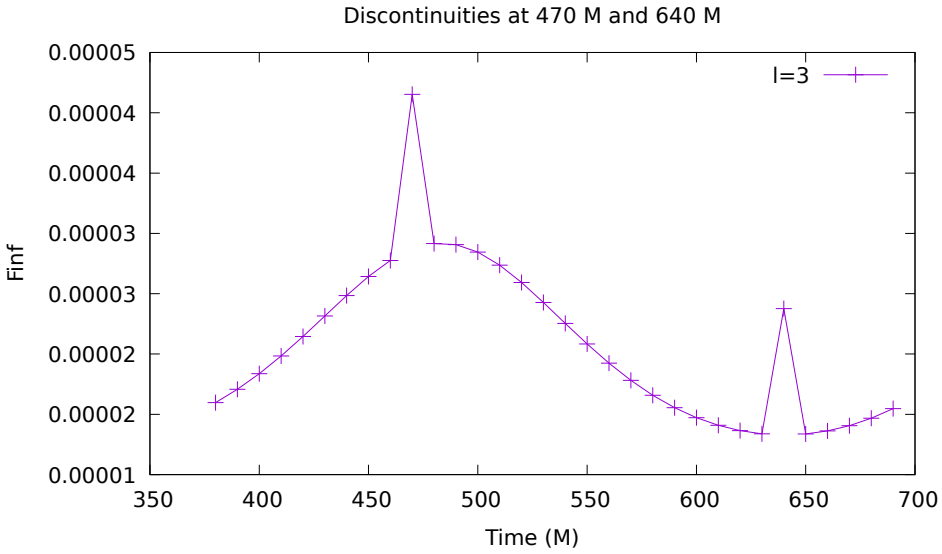
Discontinuities at 470 M and 640 M
l=3
Finf
Time (M)
0.00005
0.00004
0.00004
0.00003
0.00003
0.00002
0.00002
0.00001
350
400
450
500
550
600
650
700

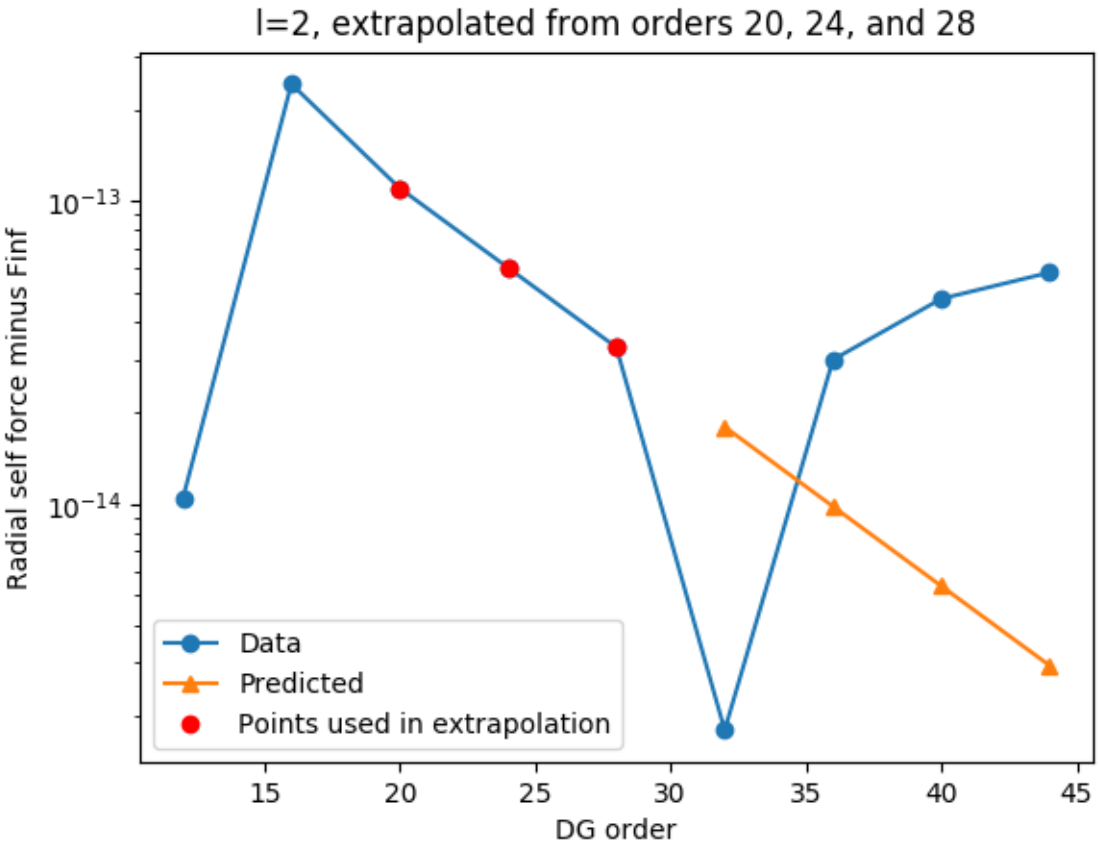
l=2, extrapolated from orders 20, 24, and 28
Radial self force minus Finf
10^{-13}
10^{-14}
DG order
15
20
25
30
35
40
45
Data
Predicted
Points used in extrapolation

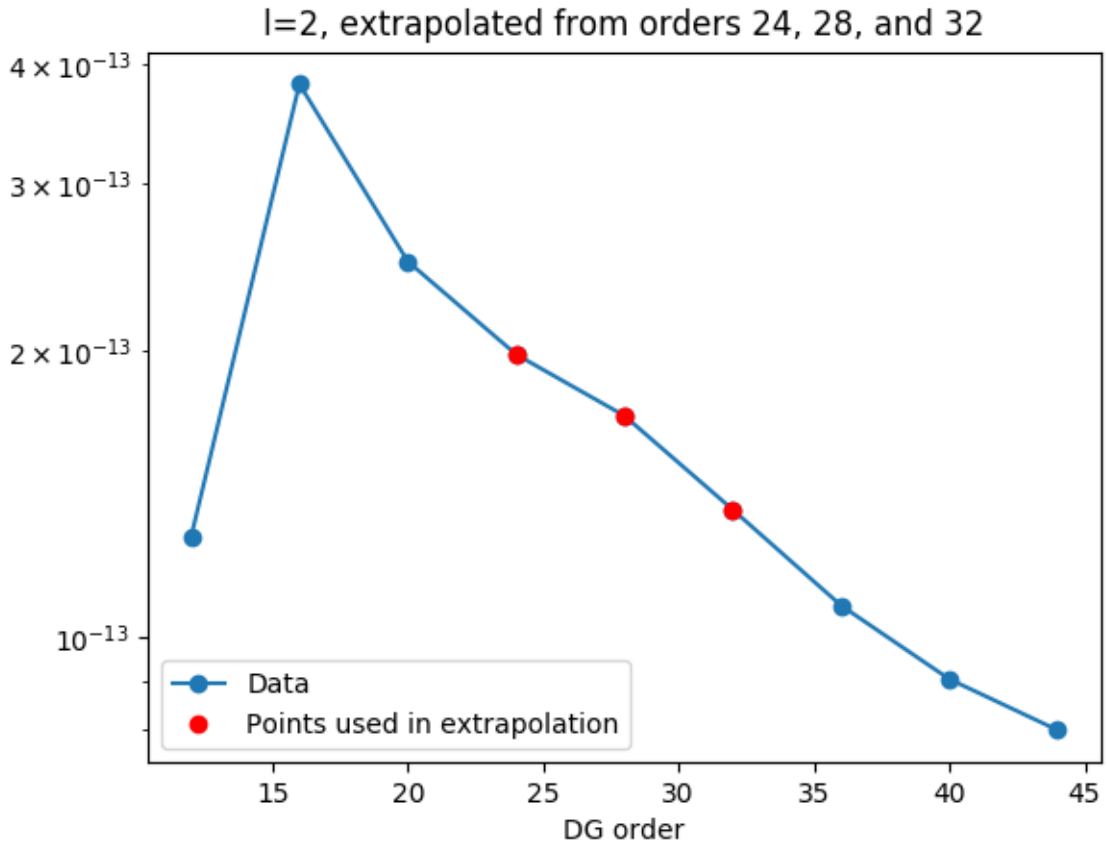

Figure 5.1: Note that the three points used in the extrapolation are not on a line on a semilog scale– it is not possible to fit an exponential through them. That is why this mode failed.

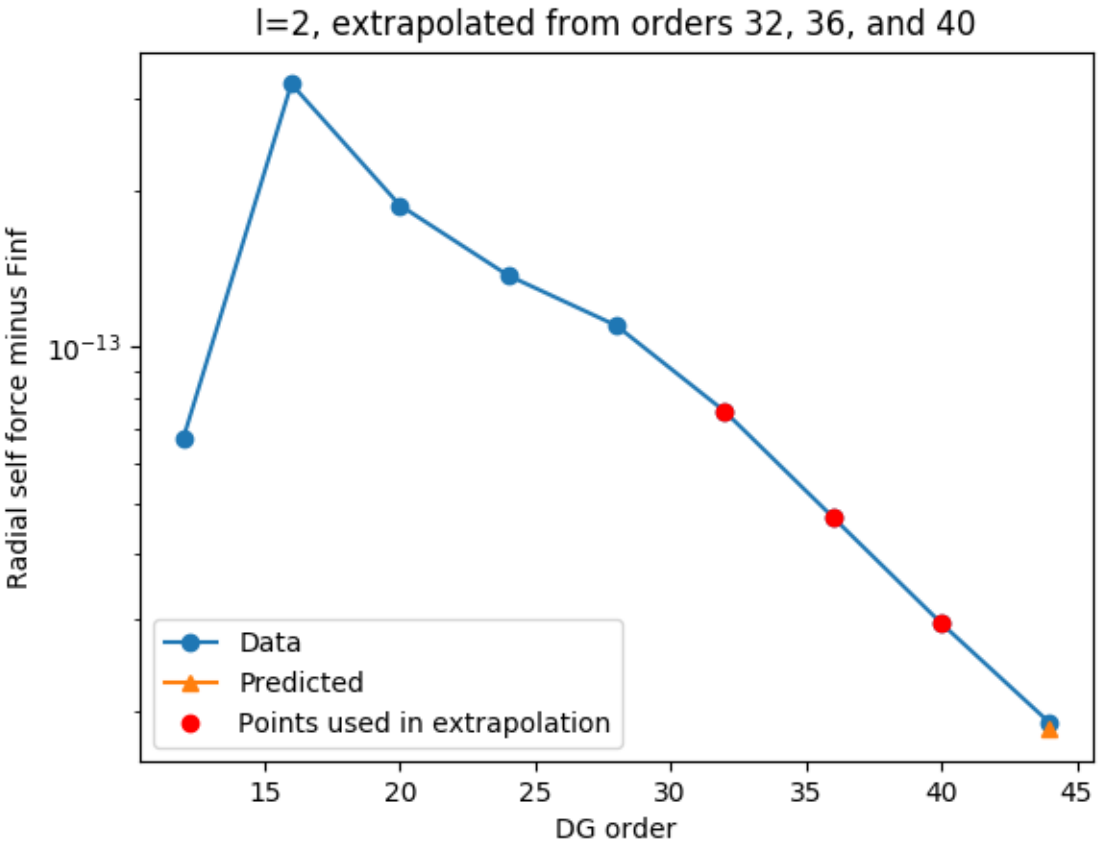
l=2, extrapolated from orders 32, 36, and 40
Radial self force minus Finf
10^{-13}
Data
Predicted
Points used in extrapolation
15
20
25
30
35
40
45
DG order

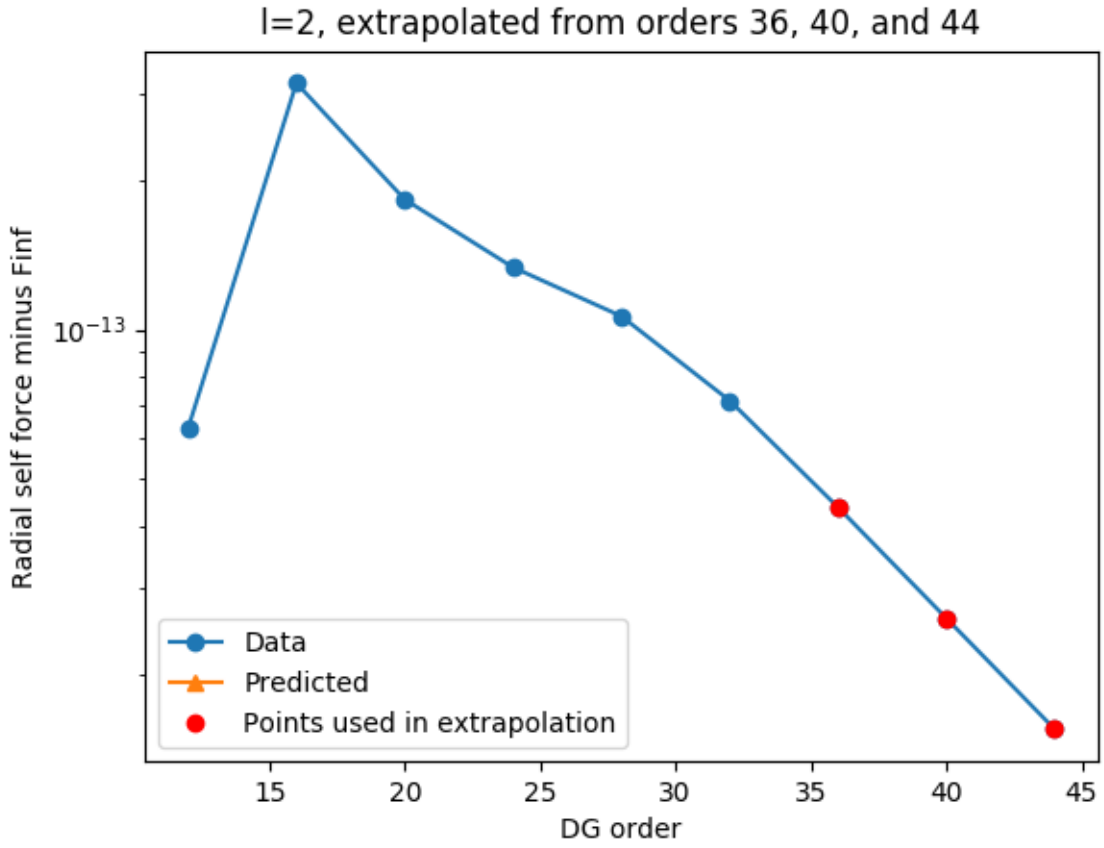
l=2, extrapolated from orders 36, 40, and 44
Radial self force minus Finf
10^{-13}
Data
Predicted
Points used in extrapolation
15
20
25
30
35
40
45
DG order

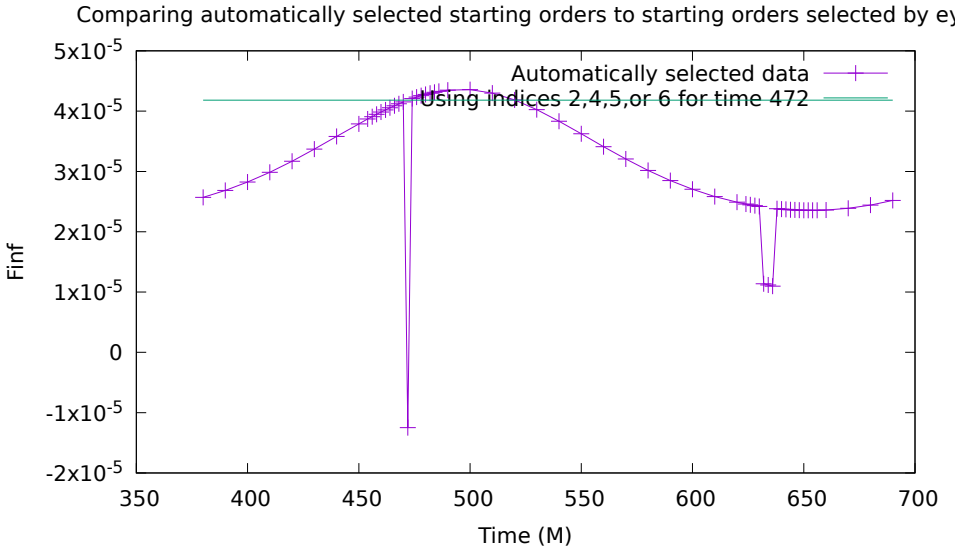
Comparing automatically selected starting orders to starting orders selected by e
Automatically selected data
Using indices 2,4,5,or 6 for time 472
Finf
5x10-5
4x10-5
3x10-5
2x10-5
1x10-5
0
-1x10-5
-2x10-5
350
400
450
500
550
600
650
700
Time (M)

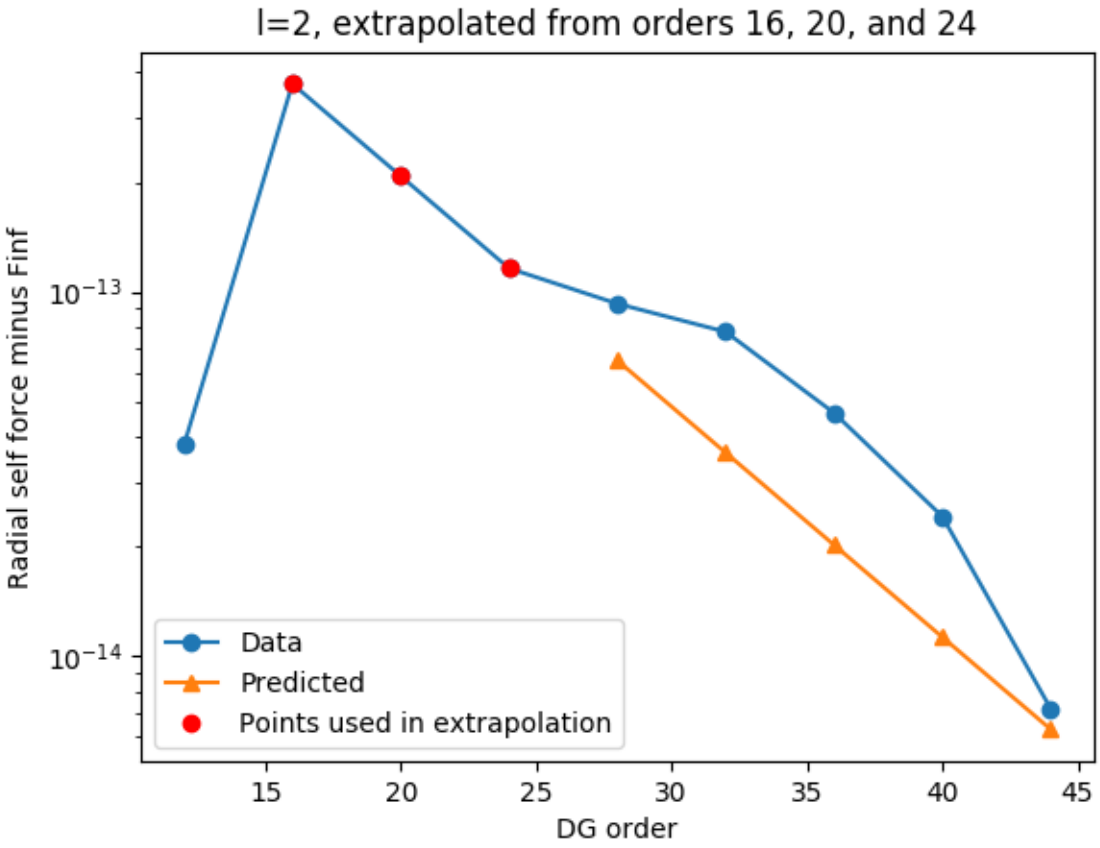
l=2, extrapolated from orders 16, 20, and 24
Radial self force minus Finf
10^{-13}
10^{-14}
Data
Predicted
Points used in extrapolation
15
20
25
30
35
40
45
DG order

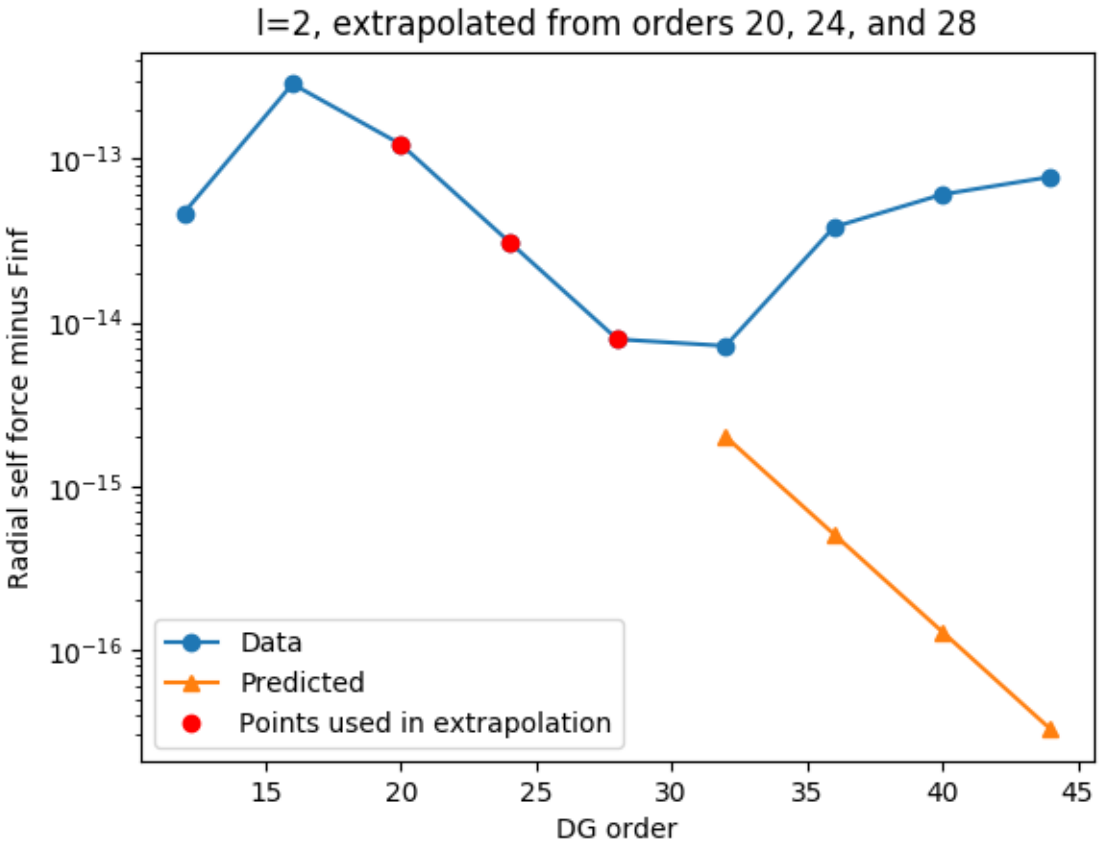
l=2, extrapolated from orders 20, 24, and 28
Radial self force minus Finf
10^{-13}
10^{-14}
10^{-15}
10^{-16}
15
20
25
30
35
40
45
DG order
Data
Predicted
Points used in extrapolation

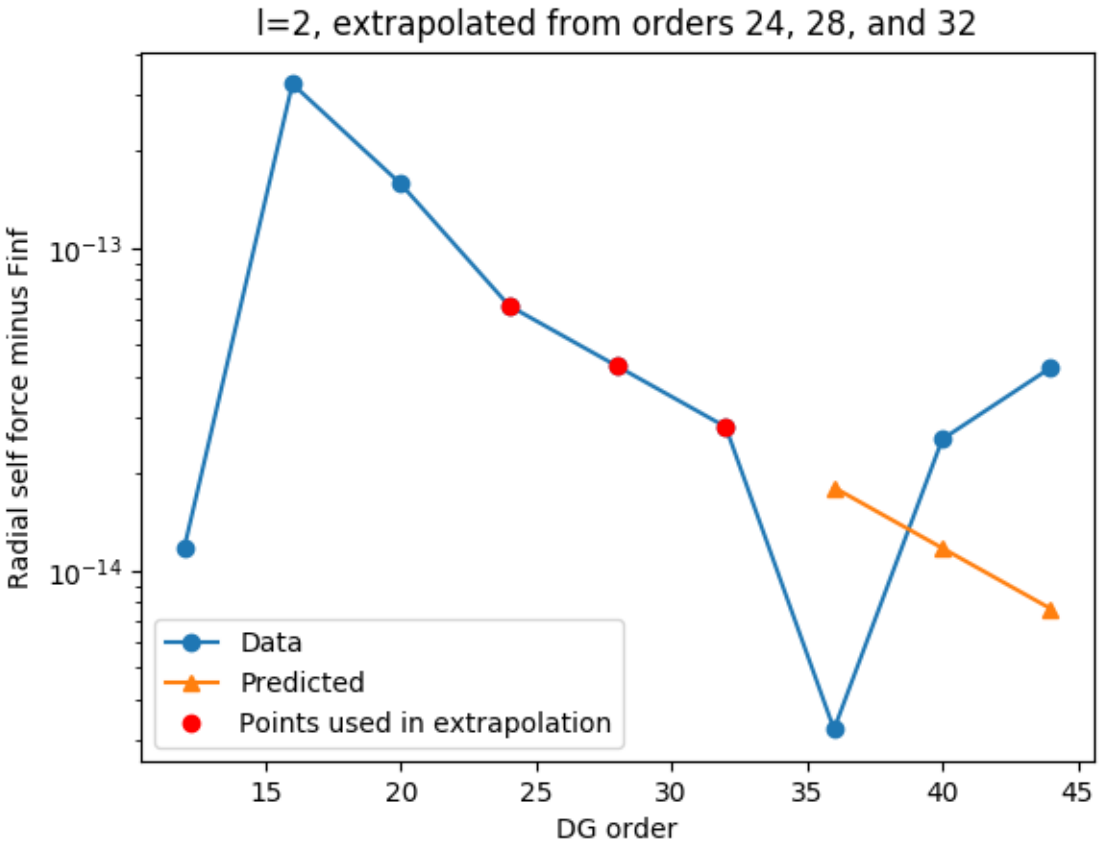
l=2, extrapolated from orders 24, 28, and 32
Radial self force minus Finf
10^{-13}
10^{-14}
Data
Predicted
Points used in extrapolation
15
20
25
30
35
40
45
DG order

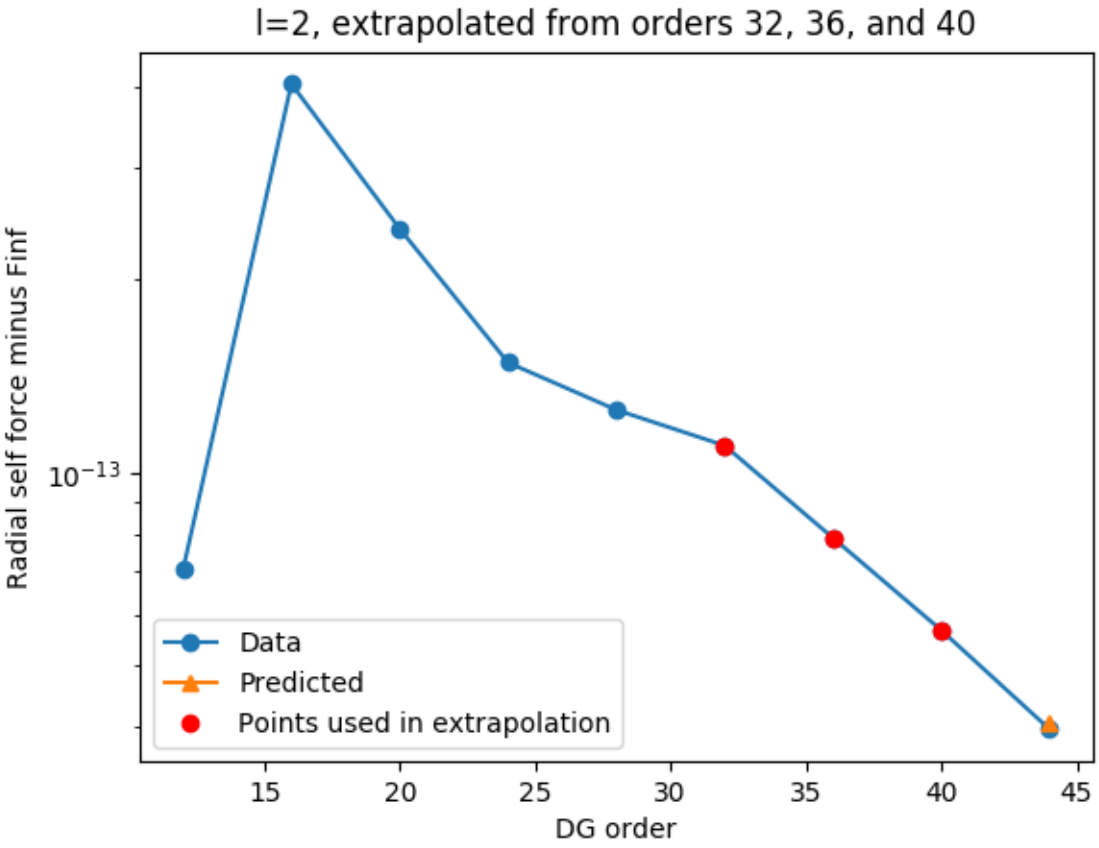
l=2, extrapolated from orders 32, 36, and 40
Radial self force minus Finf
10^{-13}
Data
Predicted
Points used in extrapolation
15
20
25
30
35
40
45
DG order

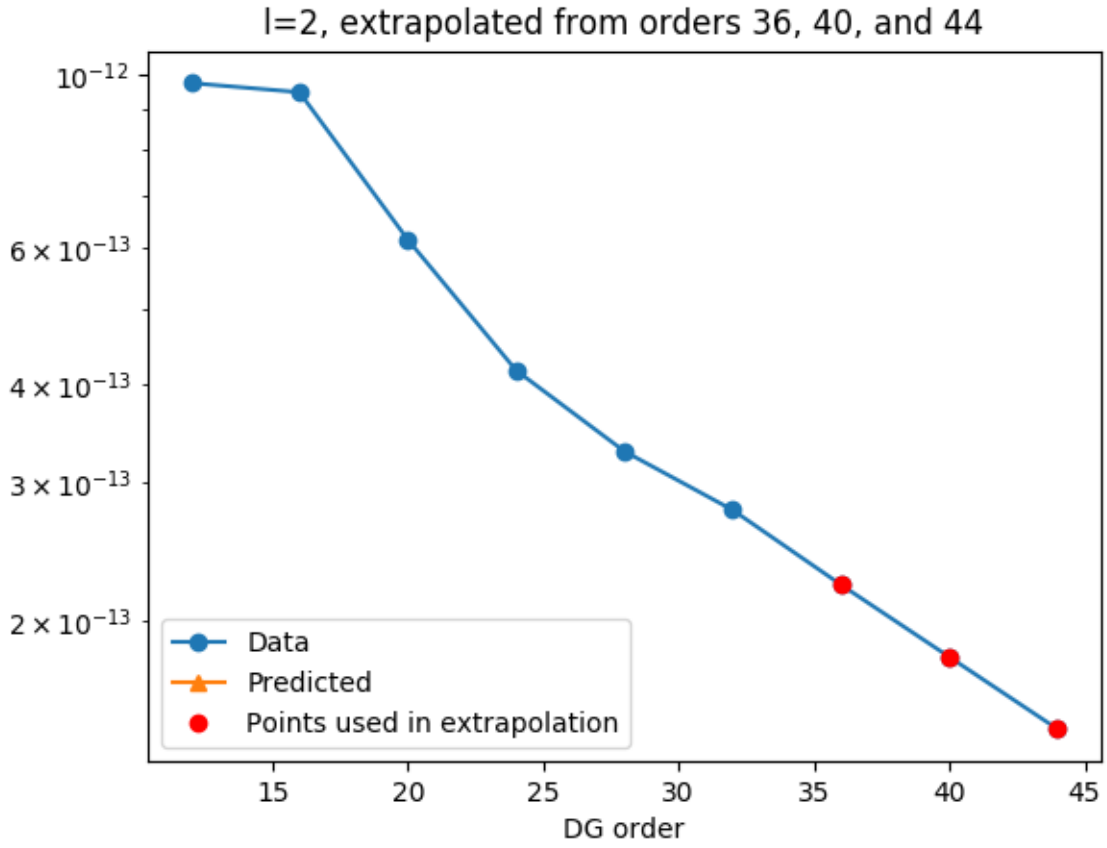
l=2, extrapolated from orders 36, 40, and 44
10^{-12}
6×10^{-13}
4×10^{-13}
3×10^{-13}
2×10^{-13}
Data
Predicted
Points used in extrapolation
15
20
25
30
35
40
45
DG order

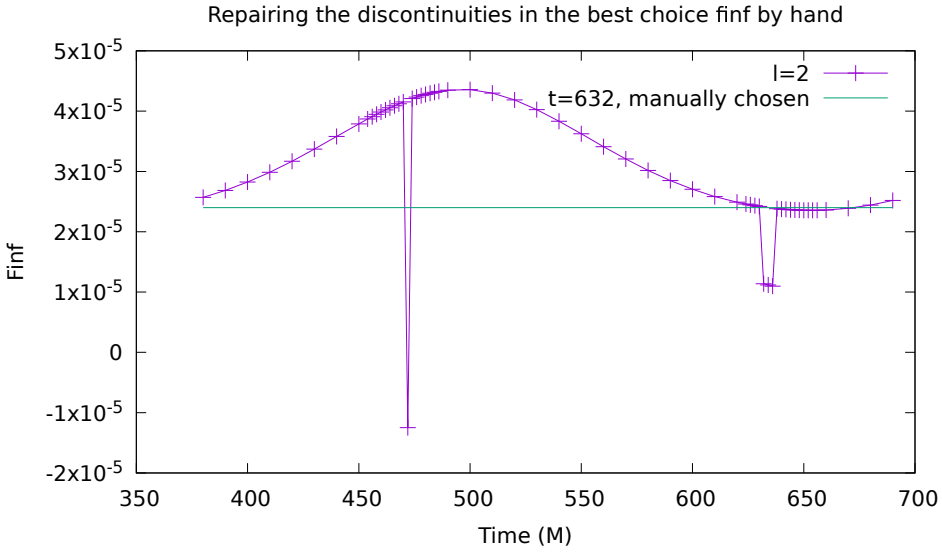
Repairing the discontinuities in the best choice finf by hand
5x10-5
4x10-5
3x10-5
2x10-5
1x10-5
0
-1x10-5
-2x10-5
Finf
l=2
t=632, manually chosen
350
400
450
500
550
600
650
700
Time (M)

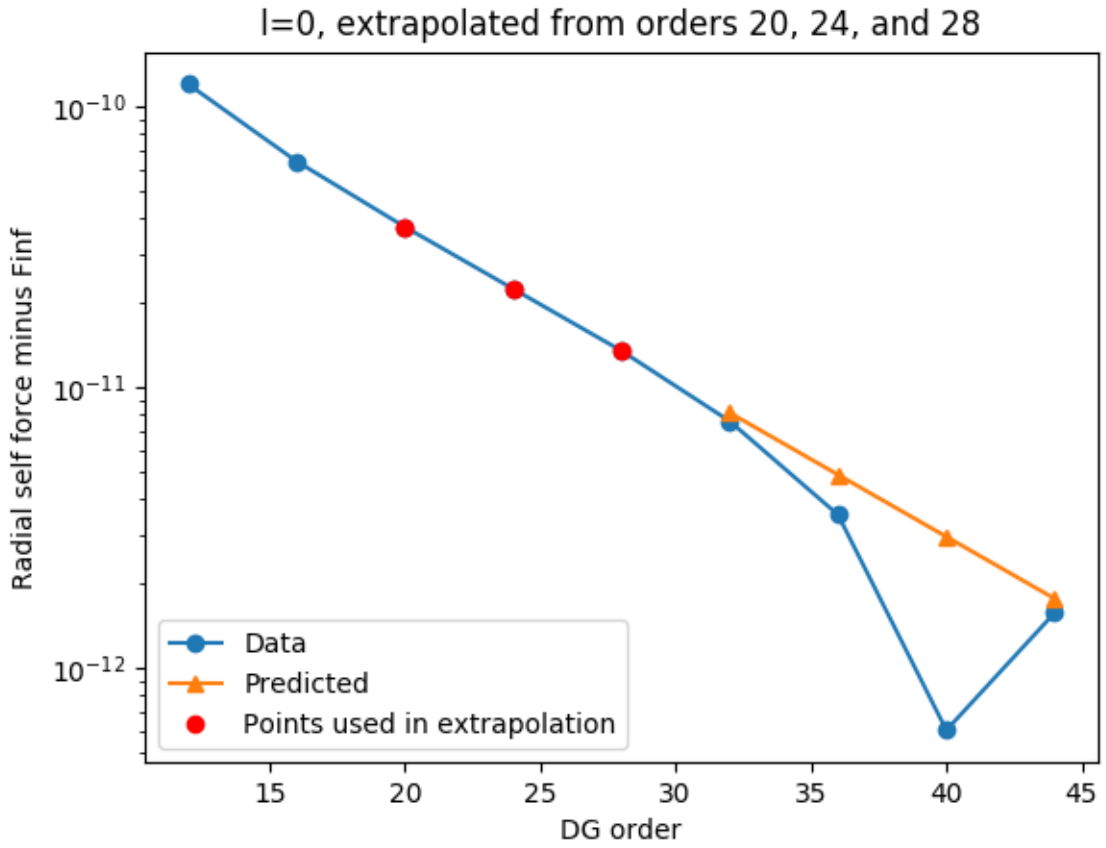

Figure 5.3: l=0 mode with fit-chosen starting index produces convergence plot with nice long exponentially converging region

time	starting order	finf
632	0	mode failed
632	1	2.40975299617e-05
632	2	2.40975300465e-05
632	3	2.40975300114e-05
632	4	mode failed
632	5	2.40975299291e-05
632	6	2.40975299148e-05
634	0	mode failed (however, 6 selected)
634	1	2.39990698129e-05
634	2	2.39990699318e-05
634	3	2.39990698774e-05
634	4	mode failed
634	5	2.39990697065e-05
634	6	2.39990696758e-05
636	0	mode failed (however, 6 selected)
636	1	2.391047416e-05
636	2	2.39104742806e-05
636	3	2.39104742249e-05
636	4	2.39104737911e-05
636	5	2.39104739924e-05
636	6	2.39104739079e-05

Chapter 6
Extrapolating the mode-summed self-force to include contributions from an infinite number of spherical harmonic modes

6.0.1 Relative error as a function of mode

We can understand why it is so hard to produce good fits by examining the relative error between different fitting techniques as a function of mode. Look at the relative error between the fit method and the median method. Both the relative and absolute error grow with l, explaining why the sigma-suppresion technique does not produce good results.

NEED SOMETHING SHOWING FIT ITSELF. NEED TO REORDER AND RECAPTION NEXT SECTION

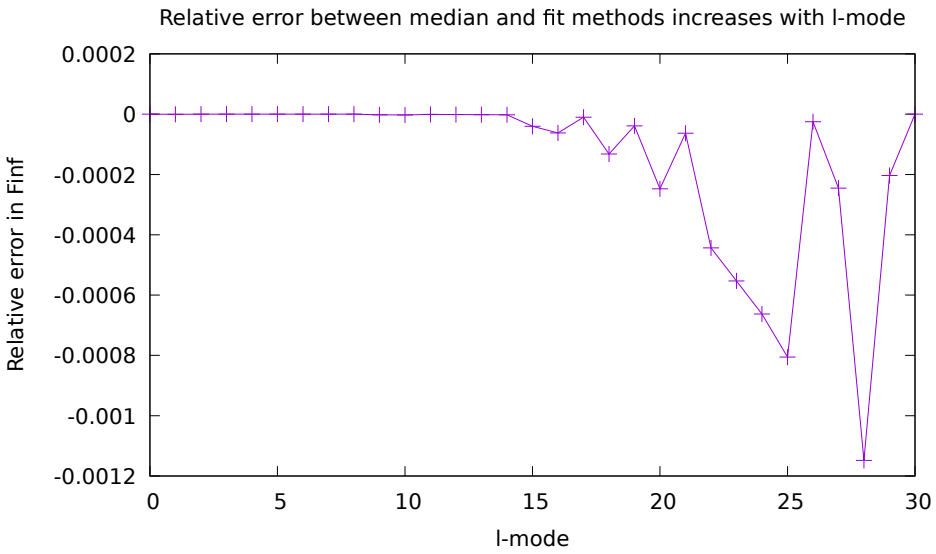

Figure 6.1: Relative error between fit and median techniques increases with l-mode

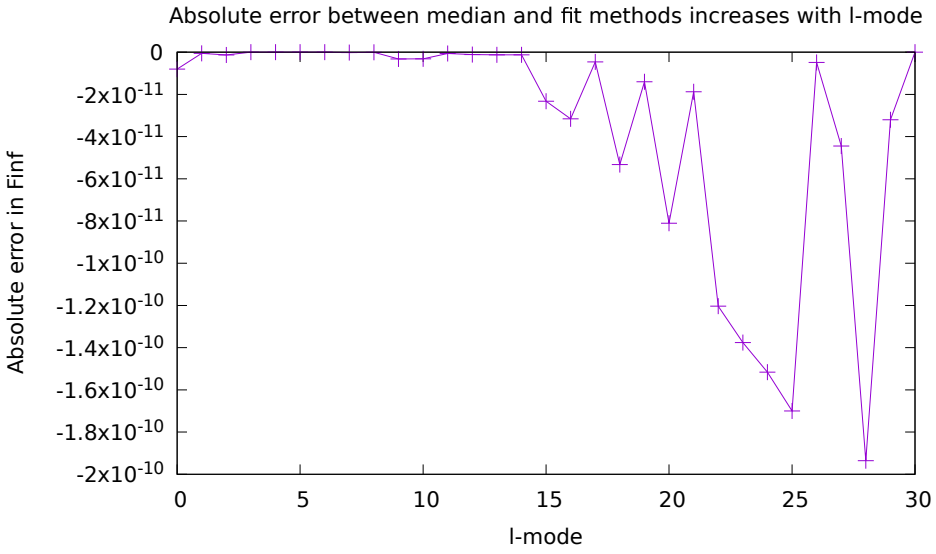

Figure 6.2: Absolute error between fit and median techniques increases with l-mode

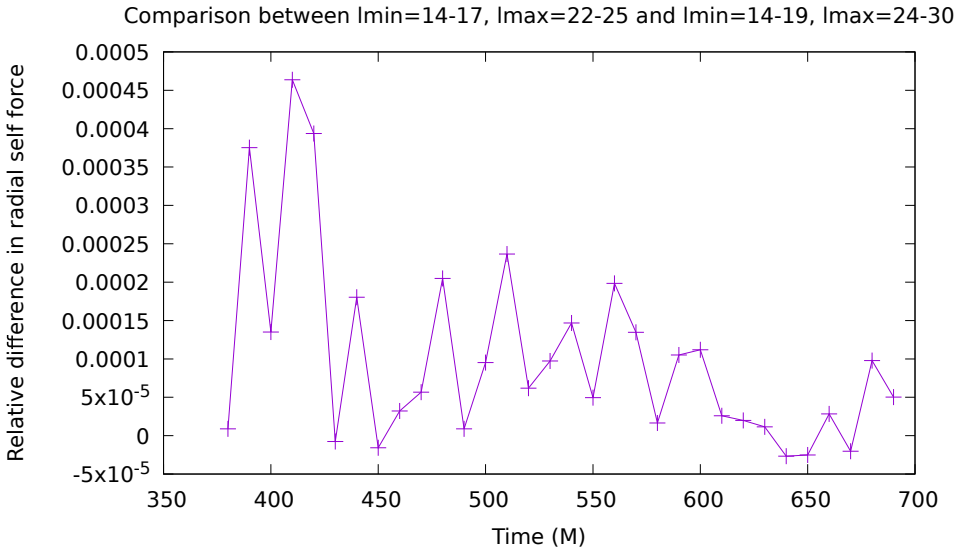

Figure 6.3: This is the relative difference between the total radial self force measured in two different ways. In both cases, the self force was extrapolated to infinite order at every l-mode at every possible DG starting order. The infinite DG order self forces over the various starting orders were sorted, eliminating NaNs. The median was chosen for each l-mode. Then the self force as a function of l-mode was fit to its three term form, and the sum was summed from zero to lmax, then extrapolated from $lmax + 1$ to infinity using an analytic form determined using Mathematica. All possible choices with lmin between 14 and 17 and lmax between 22 and 25 were averaged to obtain the total radial self force as a function of time. Similarly, all possible choices with lmin between 14 and 19 and lmax between 24 and 30 were averaged to obtain the total radial self force as a function of time. This plot shows the relative difference. I believe the smaller range is in the denominator.

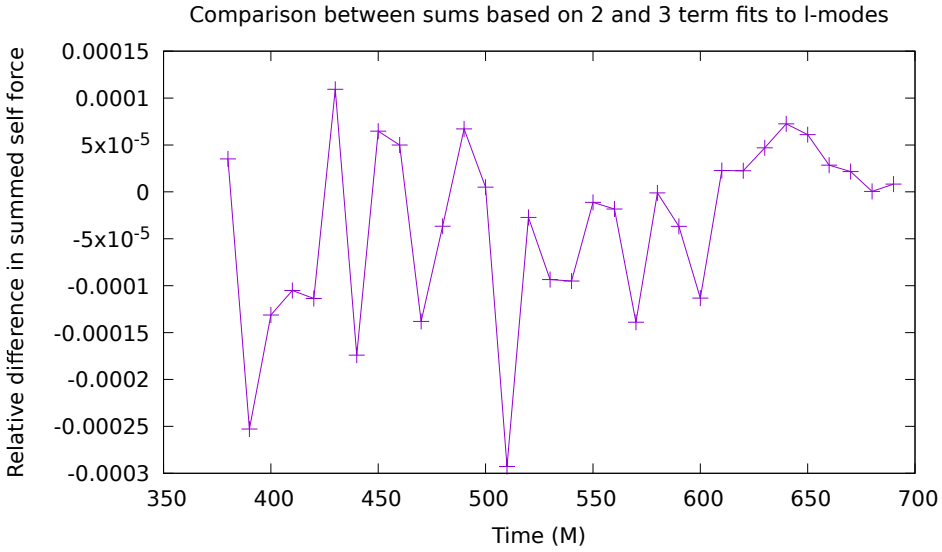

Figure 6.4: This figure was produced in the same manner as the previous figure, averaging over the smaller range, only it is a comparison between including either two or three terms in the l-mode fit. I believe the three term fit is in the denominator of the relative difference.

take standard deviation of surface plot as well as average.

6.0.2 Fractional errors

6.0.3 Structure of the error compared to the evolution in time

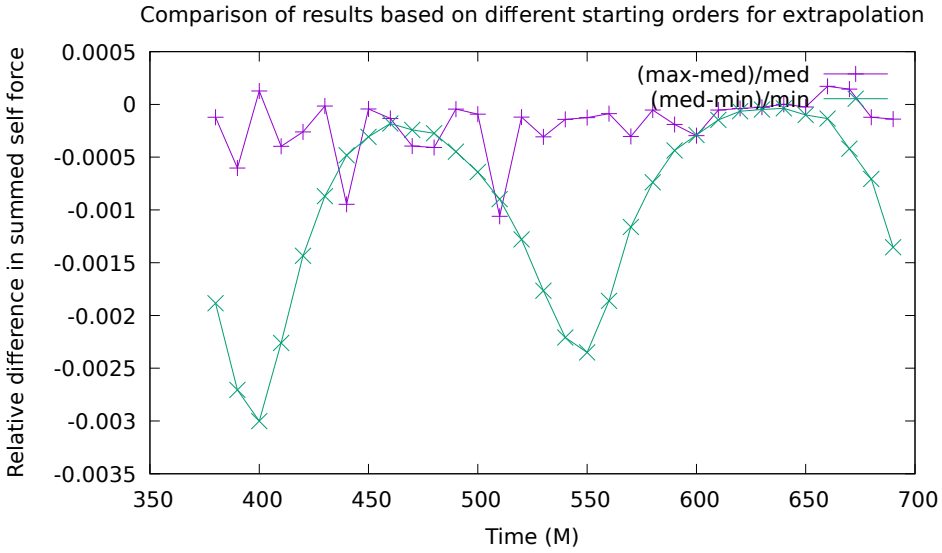

Figure 6.5: This figure was produced in a similar manner to the first figure, only instead of using the median, it is a comparison between using the median, the maximum, and the minimum. The purple line is the relative difference between the maximum and the median, which is subject to roundoff error due to the potential for the maximum to contian roundoff error. The green line is the relative difference between the median and the minimum, which is subject to effects due to failure to converge. I suspect the median is the best compromise between these two effects, rejecting outliers in both directions, though it is a simplistic approach to doing so, and does not guarantee success. It is possible to have a starting order that has not converged and is also in the roundoff regime, for example. A better guarantee of success, though not a certain one, would be to do a fit over part of the error convergence plot to determine exponentiality, by fitting a line in semilog scale. However, this seems unnecessarily complex at this time.

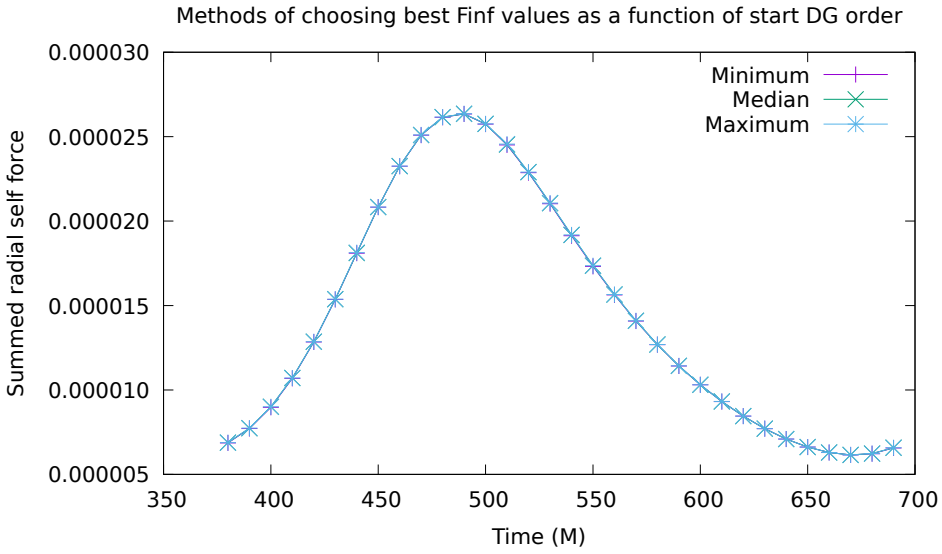

Figure 6.6: This is the actual summed, doubly extrapolated, radial self force, measured in three different ways as described in the three figures above.

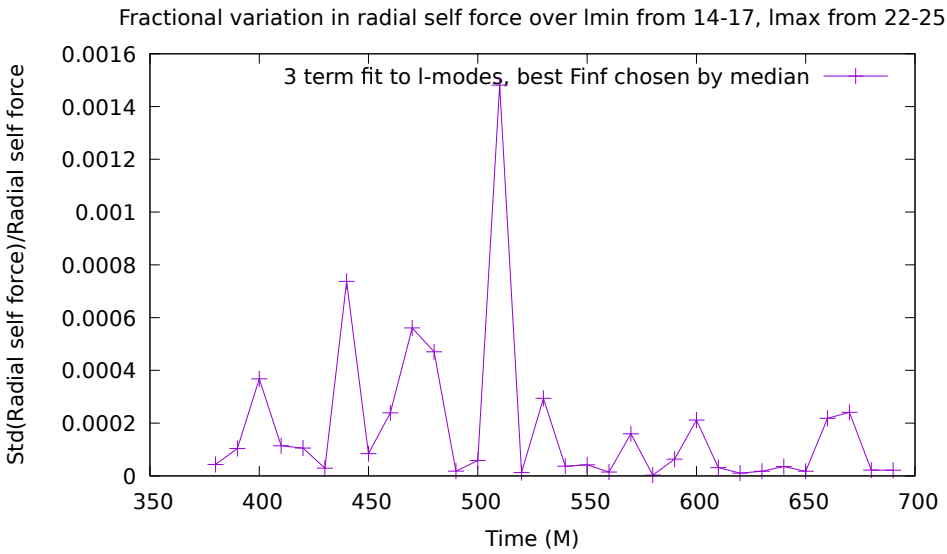

Figure 6.7: 3 term, median method

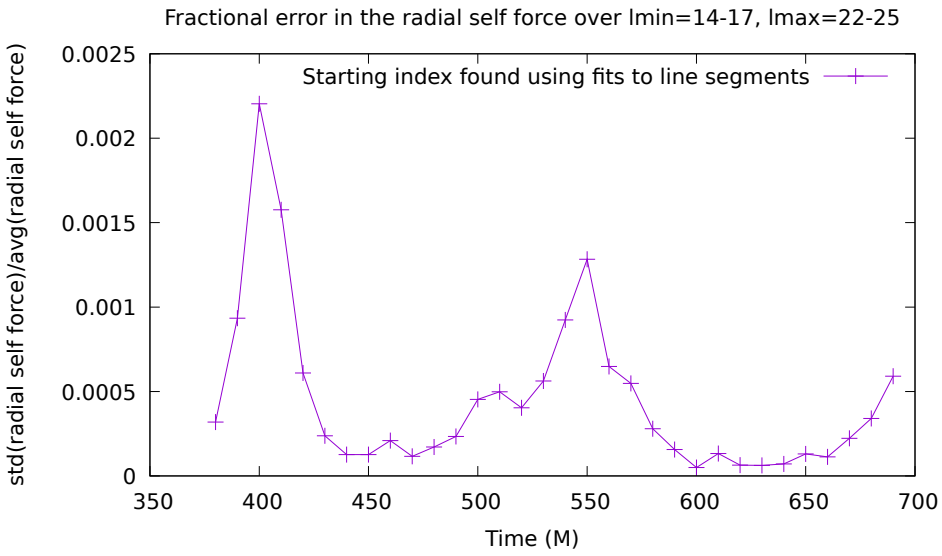

Figure 6.8: 3 term, fit method

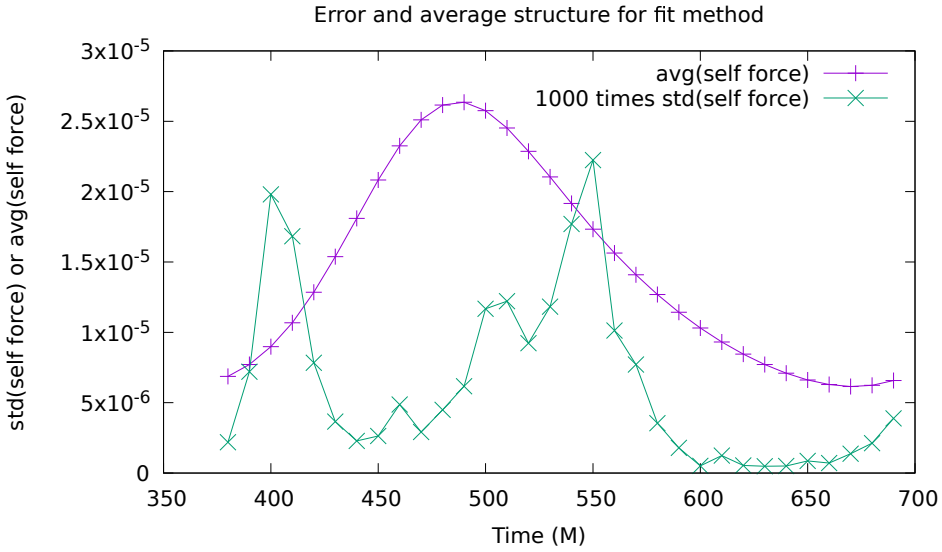

Figure 6.9: The structure of the absolute error in comparison to the evolution in time for the fit method

Chapter 7
Future work: generic orbits via the osculating orbits framework

7.1 plans for the future

going to test Peter Diener's generic orbits and help him develop them further.

7.1.1 methods

effective source osculating orbits time dependent coordinate transformation world tube already implemented with accelerated orbits though I have not run these. future work: make self consistent evolution work.

References

[1] LIGO Virgo Collaboration. (2016). Observation of Gravitational Waves from a Binary Black Hole Merger. *Phys. Rev. Lett.* 116, 061102.

[2] LIGO Virgo Collaboration. (2016). GW151226: Observation of Gravitational Waves from a 22-Solar-Mass Binary Black Hole Coalescence. *Phys. Rev. Lett* 116, 241103.

[3] LIGO Virgo Collaboration. (2017). GW120104: Observation of a 50-Solar-Mass Binary Black Hole Coalescence at Redshift 0.2. *Phys. Rev. Lett.* 118, 221101.

[4] LIGO Virgo Collaboration. (2016). Observing Gravitational-wave Transient GW150914 with Minimal Assumptions. *Phys. Rev. D* 93, 122004.

[5] LIGO Virgo Collaboration. (2016). GW150914: First Results from the Search for Binary Black Hole Coalescence with Advanced LIGO. *Phys. Rev. D* 93, 122003.

[6] LIGO Virgo Collaboration. (2016). The Rate of Binary Black Hole Mergers Inferred from Advanced LIGO Observations Surrounding GW150914. *Accepted Astrophys. J. Lett*

[7] LIGO Virgo Collaboration. (2016). Astrophysical Implications of the Binary Black-Hole Merger GW150914. *Astrophys. J. Lett* 818, L22.

[8] LIGO Virgo Collaboration. (2016). Tests of General Relativity with GW150914. *Phys. Rev. Lett.* 116, 221101.

[9] LIGO Virgo Collaboration. (2016). GW150914: Implications for the Stochastic Gravitational Wave Background from Binary Black Holes. *Phys. Rev. Lett.* 116, 131102.

[10] LIGO Virgo Collaboration. (2016). Calibration of the Advanced LIGO Detectors for the Discovery of the Binary Black-hole Merger GW150914. *Submitted to Phys. Rev. D.*

[11] LIGO Virgo Collaboration. (2016). Characterization of Transient Noise in Advanced LIGO Relevant to Gravitational Wave Signal GW150914. *Class. Quant. Grav.* 33, 134001.

[12] LIGO Virgo Collaboration and ANTARES and IceCube Collaborations. (2016). High-energy Neutrino Follow-up Search of Gravitational Wave Event GW150914 with ANTARES and IceCube. *Phys. Rev. D* 93 122010.

[13] LIGO Virgo Collaboration. (2016). GW150914: The Advanced LIGO Detectors in the Era of First Discoveries. *Phys. Rev. Lett.* 116, 131103.

[14] LIGO Virgo, ASKAP, BOOTES, Dark Energy Survey and Camera, GW-EM, Fermi GBM and LAT, GRAWITA, INTEGRAL, IPTF, InterPlanetary, J-GEM, La Silla-Quest, Liverpool Telescope, LOFAR, MASTER, MAXI, MWA, PAN-STARRS, PESSTO, PI of the Sky, SkyMapper, Swift, TAROT, Zadko, Algerian National

Observatory, C2PU, TOROS, and VISTA Collaborations. (2016). Localization and Broadband Follow-up of the Gravitational-wave Transient GW150914. *Astrophys. J. Lett.* 826, L13.

[15] Bambi, Cosimo. (2017) Testing black hole candidates with electromagnetic radiation. *Reviews of Modern Physics* 89.

[16] Martynov, D.V., et al. (2016). Sensitivity of the Advanced LIGO detectors at the beginning of gravitational wave astronomy. *Phys. Rev. D* 93, 112004.

[17] Poisson, Eric; Pound, Adam; Vega, Ian. (2011). The motion of point particles in curved spacetime. *Living Reviews in Relativity.* 14, 7.

Vita

Insert the text of your vita, which is basically a description of yourself and your academic career.